Deformation and Fracture Behavior of Polyamide Nanocomposites: The Effect of Clay Dispersion

Jiří Kotek, Ivan Kelnar, Josef Baldrian, Miroslav Šlouf

Institute of Macromolecular Chemistry, AS CR, v. v. i., Heyrovsky Sq. 2, 162 06 Prague 6, Czech Republic

Received 11 March 2008; accepted 9 June 2008
DOI 10.1002/app.28859
Published online 17 September 2008 in Wiley InterScience (www.interscience.wiley.com).

ABSTRACT: This study describes the effect of the clay content and its dispersion on deformation and fracture behavior of polyamide nanocomposites. Two nanocomposite systems, intercalated and exfoliated nanocomposites containing layered silicate, were compared. They were prepared by melt-compounding of polyamide with sodium montmorillonite or organophilized montmorillonite. It has been shown that while the exfoliated structure imparts to the nanocomposite higher stiffness and strength, the toughness is inferior to the intercalated nanocomposite. © 2008 Wiley Periodicals, Inc. J Appl Polym Sci 110: 3752–3757, 2008

Key words: polyamide nanocomposite; toughness; montmorillonite; intercalation; exfoliation

INTRODUCTION

Polymer/layered-silicate nanocomposites represent a radical alternative to conventional microcomposites. They exhibit improved stiffness and strength as well as supressed thermal expansion coefficients and enhanced barrier properties. In recent years, the concept has been used to prepare nanocomposites based on various engineering polymers including epoxies, unsaturated polyesters, poly(ε-caprolactone), poly(L-lactide), poly(ethylene oxide), silicon rubber, polystyrene, polyamide, polypropylene, polyethylene, poly(ethylene terephthalate), polyurethane, and polybutene (Refs. 1–3 and references therein).

A majority of nanocomposite studies have focused on the effects of the clay surface treatment and concentration on various aspects of these materials. However, the knowledge of the deformation and fracture mechanisms of nanocomposites is rather vague. Only few studies have provided comprehensive reports of the fracture behavior of nanocomposites. Zilg et al.[4] compared the balance of toughness/stiffness in a variety of epoxy/layered silicate composites with different extents of exfoliation, that is, conventional, intercalated, and exfoliated systems. They suggested that the exfoliated structure leads to an improved modulus, whereas the remaining stacked structure of intercalated clay platelets is the key to improving toughness. Platelets are proposed to produce nanovoids and initiate shear yielding of the epoxy interlayers at the tip of the propagating crack and also in the bulk. These mechanisms, however, are only speculations as no direct evidence was presented. Wang et al.[5] showed that the initiation and development of microcracks is the dominant in microdeformation and fracture mechanisms in epoxy/clay nanocomposites. Most microcracks initiated between the clay layers, which developed within tactoids and extended into the matrix with increasing strain. The microcracks tend to penetrate through the matrix ligaments and merge leading finally to catastrophic fracture. The formation of a large number of microcracks and the increase in fracture surface area due to crack deflection are suggested to be the major toughening mechanisms. On the other hand, Kinloch and Taylor[6] noticed that the fracture toughness of the epoxy/clay nanocomposite is lower than that of microcomposites. In fact, the thermoset nanocomposites are the only systems where increased toughness was observed.

Generally, toughness is the only mechanical parameter of polymeric nanocomposites that is not enhanced, but even decreased. Moreover, it seems that possible fracture toughness enhancements are system-specific, and thus no systematic predictive methodologies have been developed. Chen et al.[7] characterized toughness of maleated polypropylene/clay nanocomposites using the *J*-integral fracture mechanics approach. They observed a reduction in ductility and toughness as a result of the constrained mobility of polymer chains in the vicinity of clay surface. Nathani et al.[8] showed that combining polybutene with 5 wt % clay alters the primary micromechanism of

Correspondence to: J. Kotek (kotek@imc.cas.cz).
Contract grant sponsor: Academy of Sciences of the Czech Republic (project B200500601).

stress whitening from stress relaxation of tiny voids and subsequent transformation to ridge tearing at high plastic strains to nucleation and growth of large-size voids in polybutene-clay nanocomposites. The final fracture in neat polybutene occurred by a mixed mode (brittle fracture and fibrillation), whereas brittle deformation was the predominant fracture mode in polybutene/clay nanocomposites. Gloaguen and Lefebvre[9] showed that significant microvoiding is associated with the clay nano-reinforcement in polyamide 6 nanocomposites. They showed that while shear-banding accounts for more than 90% of the plastic deformation in neat polyamide, in the nanocomposite at least 45% of the deformation is of cavitational nature. Nair et al.[10] reported that the multiscale structure, that is, mixture of exfoliated and micron-size particulate clays, of polyamide-6,6/clay nanocomposites is favorable to toughening. This combines toughness from the nanodispersed clay with crack propagation resistance originating from the micrometer-sized particles. Yu et al.[11] observed a decrease in ductility and fracture toughness of polyamide-6,6 in the presence of exfoliated clay. With increasing clay content the fracture toughness further decreased. Kim et al.[12] studied deformation mechanisms of polyamide 6/clay nanocomposites prepared by melt compounding of polyamides with different molecular weight with the clay. They observed that the degree of clay dispersion increases with increasing molecular weight of the matrix. Although low-molecular-weight polyamide formed intercalated morphology, the clay was well exfoliated in high-molecular-weight polyamide. The same authors confirmed that the presence of layered silicate induces the crystallization of polyamide in the γ-phase, predominantly at the silicate surface, whereas the α-phase occurs in the bulk. This is in agreement with other observations.[13] Kim et al.[12] proposed a deformation model based on the fact that the exfoliated structure exhibits higher proportion of the γ-phase, which leads to stronger polymer–clay interactions. These interactions provide an energetic barrier to phase separation and debonding. Thus, the prominent deformation mechanism is cavitation inside the intercalated tactoids and/or at the vicinity of the clay in the matrix.

On the basis of the literature data, it seems that a fully exfoliated nanocomposite does not lead itself to certain toughening mechanisms in view of the length scale and size arguments. Nanoscale reinforcements are by orders of magnitude smaller than the fracture process zone in the crack tip region. Crack-tip blunting, which takes place in microcomposites, is not possible in the case of nanoscaled fillers with sizes smaller than the radius of gyration of polymer chains. On the other hand, it has also been suggested that the increase in the clay surface area due to the size effect can contribute to enhanced shear plasticity provided interfacial adhesion is sufficient and the clay layers are suitably aligned.[10] As a result, the increase in plastic deformation is expected to be larger with decreasing scale of reinforcement. In other words, fully exfoliated structures should be favorable to toughening. The basic reason for the synergistic improvement in properties is still far from being understood. The current thinking is that nanoparticle effects are related to confined polymer matrices, originating from ultrafine sizes, morphology, and interfacial interactions of the phases involved. The extremely high surface-to-volume ratio of the clay layers, and presumably the strong polymer chain linkage to the clay surface cause unexpected changes in molecular dynamics. The confined polymer chains close to nanofiller particles are immobilized, which causes a shift of glass-transition temperature (T_g) to higher temperatures. At the same time, the enhanced chain mobility at the surface is the reason of reduced T_g occurring in thin polymer films, porous materials (microcellular), and in some cases in composites with poor interfacial adhesion.[14] In the last case, the depression of T_g was related to the enhanced polymer dynamics due to extra free volume at the filler/matrix interface, and it depends significantly on clay–polymer interactions.[15] Because of the counteraction of both these effects, it is not surprising that both decreases[16,17] and increases[11,18] in glass-transition temperature in nanocomposites have been reported.

The aim of this study is to describe the effect of clay dispersion on deformation and fracture behavior of polyamide nanocomposites. Polyamide 6/clay nanocomposites with different morphology (differing in the degree of clay delamination) were prepared. This was achieved by melt-compounding of polyamide with sodium montmorillonite and organophilized montmorillonite. This approach made it possible to compare nanocomposites with the same inorganic content but differing in morphology.

EXPERIMENTAL

Materials

A commercial-grade polyamide 6 (PA6) Ultramid B4 (BASF, Germany) was used as the matrix. The material is characterized by a number–average molecular weight M_n of $\sim$ 33,000. Two commercial types of nanoclay based on natural montmorillonite were used: sodium montmorillonite Cloisite Na+ (CNa) and montmorillonite modified with alkylbis (2-hydroxyethyl) methylammonium chloride, the alkyl being derived from tallow, Cloisite 30B (C30). Both clays are commercial products supplied by Southern Clay Products, USA.

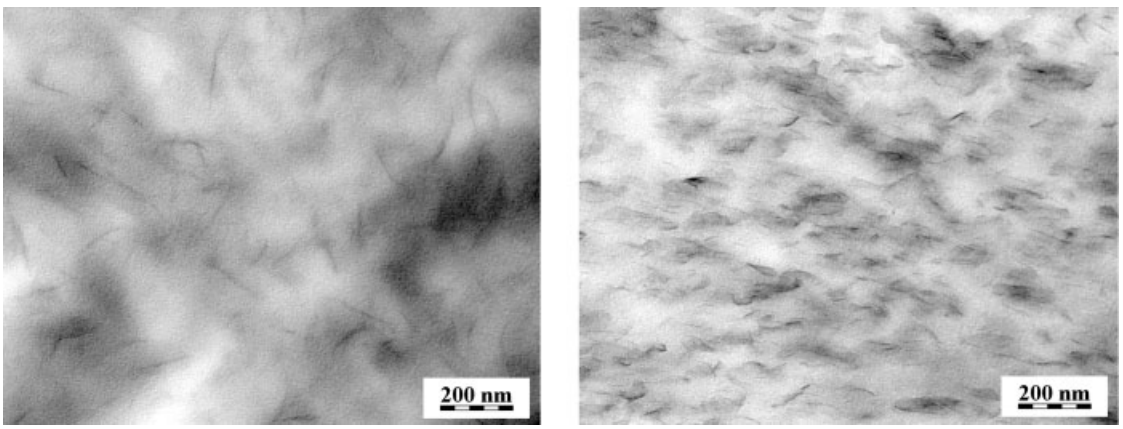

Figure 1 TEM micrographs of nanocomposites with 1 wt % (left) and 5 wt % (right) of CNa.

Sample preparation

Prior to mixing, PA6 and clay were dried at 85 and 70°C, respectively, for 12 h in a vacuum oven. Nanocomposites were prepared by mixing the components in a Brabender DSE 20 twin-screw corotating extruder (diameter 20 mm, length/diameter = 40) at 500 rpm, the temperatures of heating zones being 260, 260, 270, 270, 270, and 275°C. Dumbbell specimens (type 1A according to ISO 527 standard) were injection-molded using a Battenfeld BA 100 injection molding machine. The barrel zone temperatures were 270, 275, 280, and 275°C, the temperature of the mold was 80°C. For fracture toughness determination, bars with thickness $B = 4$ mm, width $W = 10$ mm, and length $L = 60$ mm were cut from central part of the dumbbell specimens.

Structure characterization

X-ray diffraction (XRD) studies were carried out to evaluate the degree of clay delamination. Wide-angle X-ray diffraction patterns (WAXS) were obtained using a powder diffractometer HZG/4A (Freiberger Präzisionsmechanik, Germany) and monochromatic CuKα radiation. The diffractograms were scanned in the 2Θ range from 1.4 to 10°. XRD was used also for the assessment of crystallinity and γ-form content. The proportion of the γ-form within the crystalline phase was calculated with help of integral intensities of α- and γ-forms obtained using peak deconvolution program applied to the diffraction patterns of studied samples.

Ultrathin sections for transmission electron microscopy, ~ 40-nm thick, were cut with Leica Ultracut UCT ultramicrotome equipped with cryo attachment. Temperatures during cutting were −110°C and −50°C for the sample and a knife, respectively. Transmission electron microscopy (TEM) was performed with microscope JEM 200CX (JEOL, Japan). All TEM micrographs were taken at the acceleration voltage 100 kV, recorded on a photographic film and digitized with a PC-controlled digital camera DXM1200 (Nikon, Japan).

Testing

Tensile testing was performed at room temperature using an Instron 5800 testing machine according to the ISO 527 standard. The cross-head speed was 50 mm/min except for the Young's modulus determination, which was carried out at a cross-head speed of 1 mm/min.

An instrumented Charpy impact tester PSW 4 with 4 J work capacity was used for the *J*-integral evaluation. Experimental parameters were: notch depth $a = 2$ mm ($a/W = 0.2$); support span $s = 40$ mm ($s/W = 4$); pendulum hammer speed $v_H = 1.5$ ms^{-1}. During impact tests the load (F) deflection (f) diagrams were recorded. The total deformation energy up to the maximum impact load (A_G) was divided into elastic (A_{el}) and plastic (A_{pl}) parts. The values of the *J*-integral were determined using eq. (1), proposed by Sumpter and Turner[19]:

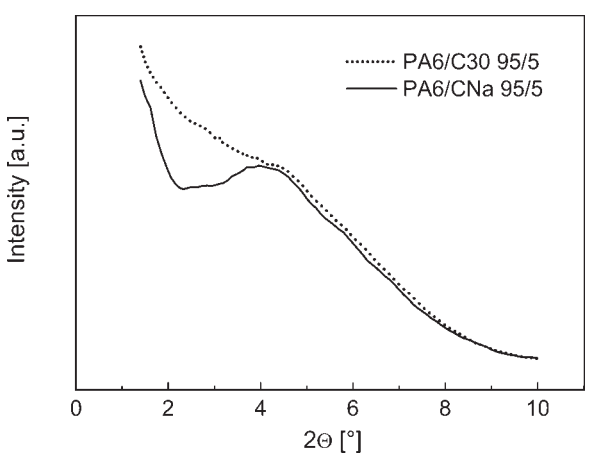

Figure 2 X-ray diffraction curves of nanocomposites with 5 wt % of the clay.

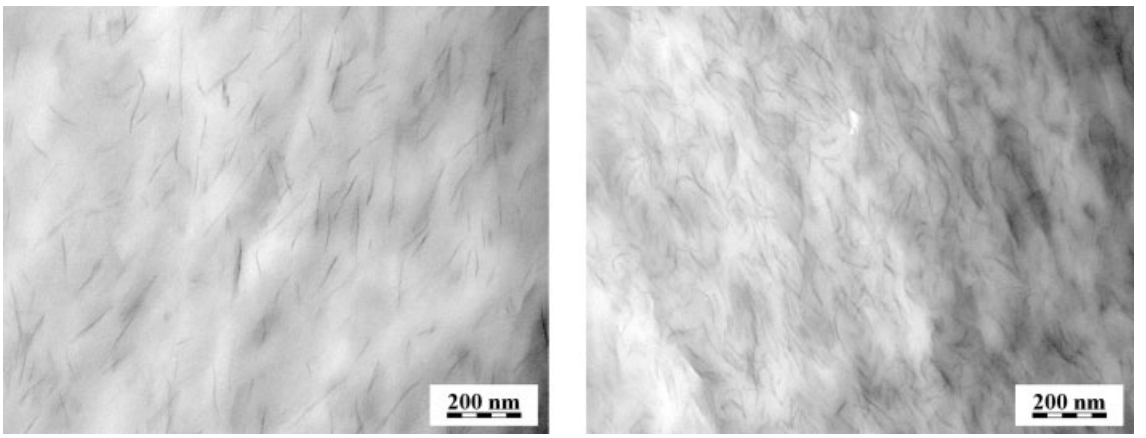

Figure 3 TEM micrographs of nanocomposites with 1 wt % (left) and 5 wt % (right) of C30.

$$J_{Id}^{STEA} = \eta_{el}\frac{A_{el}}{B\,(W-a)} + \eta_{pl}\frac{A_{pl}}{B\,(W-a)}\frac{W-a_{eff}}{W-a} \quad (1)$$

where

$$\eta_{el} = 0.5 + 5.5\,(a/W) - 5\,(a/W)^2 \quad (2)$$

$$\eta_{pl} = 2 - \frac{(1-a/W)(0.892 - 4.476\,a/W)}{1.125 + 0.892\,(a/W) - 2.238\,(a/W)^2} \quad (3)$$

and a_{eff} is the crack length at the onset of unstable crack propagation measured using a light microscope equipped with a metering table.

The reported values of all mechanical parameters are averages of 10 measurements.

RESULTS AND DISCUSSION

Structure

The clay delamination was elucidated using TEM and XRD. In XRD patterns the interlayer spacing of clay was determined from the 2Θ position of the peak corresponding to the {001} basal reflection of montmorillonite (referred to as d_{001} peak). The original organoclays Cloisite Na+ and 30B exhibit the gallery distance 1.17 and 1.85 nm, respectively. The chemical nature of clay surface is particularly imprinted in the resulting clay dispersion in the matrix. TEM revealed that the sodium-exchanged clay CNa forms mainly intercalated structures, with certain amounts of exfoliated platelets, as is demonstrated in Figure 1 for the nanocomposite containing 5 wt % of the clay. The corresponding XRD trace in Figure 2 exhibits a reflection peak at $2\Theta = 4^\circ$, related to the d_{001} basal spacing of 2.2 nm. Compared with the value of pristine CNa clay, the d_{001} spacing is increased by $\sim$ 1 nm. The shoulder position as well as the structure observed by TEM, seems to be independent on clay content within the applied clay concentrations. Organophilized C30 platelets are well exfoliated in the matrix, Figure 3. However, there are some stacks consisting of several platelets, which resulted in a slight shoulder on the XRD curve at 2Θ position, corresponding to the interlayer spacing d_{001} $\sim$ 2.2 nm, Figure 2. Again, the clay dispersion does not change with the used clay content.

Although XRD reflections in the low-angle region ($2\Theta \leq 10^\circ$) gave information on basal spacing between individual silicate layers, an inspection of XRD traces in the wide-angle region ($2\Theta \geq 10^\circ$) predicate of the phase structure of the polyamide matrix. It has been shown that the clay has a decisive γ-nucleation effect. The values of crystallinity X_c and proportion of the γ-form within the crystalline phase are summarized in Table I. The higher γ-form content in exfoliated nanocomposites corresponds to the fact that this form is preferentially formed in the vicinity of the silicate surface, whereas the α-form exists farther from the polymer-silicate region.[13]

TABLE I
Degree of Crystallinity and the γ-Form Content in the Crystalline Phase

	Skin (reflexion mode)		Cross-section (transmission mode)	
Sample	X_c (%)	γ-form (%)	X_c (%)	γ-form (%)
Neat PA6	27	78	29	36
PA6/CNa 99/1	45	97	31	42
PA6/CNa 97/3	42	97	28	45
PA6/CNa 95/5	43	97	25	55
PA6/C30 99/1	45	97	25	55
PA6/C30 97/3	42	97	28	52
PA6/C30 95/5	40	97	24	55

TABLE II
Mechanical Properties of Studied Materials: Young modulus, *E*, Tensile Strength, σ_M, Strain at Tensile Strength, ε_M, and Strain at Break, ε_b

Sample	*E* (MPa)	σ_M (MPa)	ε_M (%)	ε_b (%)
Neat PA6	2930 ± 170	73.2 ± 1.9	4.4 ± 0.3	120 ± 40
PA6/CNa 99/1	3370 ± 115	87.0 ± 0.2	4.2 ± 0.2	23.0 ± 6.0
PA6/CNa 97/3	4060 ± 175	94.0 ± 0.9	4.3 ± 0.1	8.0 ± 1.2
PA6/CNa 95/5	4530 ± 135	96.8 ± 0.3	4.3 ± 0.1	8.6 ± 1.6
PA6/C30 99/1	3450 ± 140	87.3 ± 0.2	4.4 ± 0.3	22.4 ± 5.1
PA6/C30 97/3	4780 ± 175	99.5 ± 0.7	4.3 ± 0.3	6.7 ± 1.8
PA6/C30 95/5	6030 ± 280	97.5 ± 1.9	4.4 ± 0.6	4.4 ± 0.6

Mechanical behavior

The following mechanical characteristics were derived from the stress–strain diagrams: Young modulus, *E*, tensile strength, σ_M, strain at tensile strength, ε_M, and strain at break, ε_b. All experimental data are summarized in Table II. It can be seen that the presence of the clay strongly affects tensile mechanical properties. Although the neat polyamide exhibits cold drawing beyond the yield point and its strain-at-break is ~ 120%, the clay significantly influences the failure mode. 1 wt % of CNa reduces the ultimate strain to 23%. The strain-at-break value then further decreases, again with increasing filler content. The nanocomposites containing 3 and 5 wt % fail immediately after reaching the yield point at the strain-at-break value of ~ 8%. The tensile behavior of nanocomposites with exfoliated C30 clay is similar. Again, the presence of 1 wt % of the clay reduces the strain at break to about 22% and increasing filler content changes semiductile behavior to brittle fracture. Moreover, the higher amount of immobilized chains in exfoliated nanocomposites leads to slightly lower values of ultimate strain. Indeed, the nanocomposite with 5 wt % of C30 breaks before reaching the yield point, which manifests itself not only in equal values of ε_M and ε_b, but mainly in lower value of strength in comparison with the same system containing 3 wt % of clay.

The presence of clay enhances both tensile modulus and tensile strength, Figure 4. It seems that the Young modulus values are in good agreement with the clay content and degree of its dispersion. First, the stiffness increases with increasing clay content. Second, a significantly higher increase in Young modulus is observed for the exfoliated system with C30. Also tensile strength is markedly enhanced by the clay. It increases from 73 MPa for neat polyamide to ~ 87 MPa for the systems containing 1 wt % of clay. At this loading level, there is no difference between exfoliated and intercalated systems. This can be ascribed to the competing effect between clay reinforcement on one hand and the crystalline structure on the other. Even though the exfoliated clay increases strength more efficiently than the intercalated one, the intercalated nanocomposite has a considerably higher crystallinity and higher proportion of the α-form, which is more rigid than the γ-form[20] which prevails in exfoliated nanocomposite. At a higher clay content (3 wt %), the exfoliated nanocomposite with C30 exhibits a significantly higher strength than the intercalated counterpart. Although the strength of intercalated system further increases, the tensile strength of the exfoliated nanocomposite containing 5 wt % of C30 slightly decreases. It is a consequence of low ductility and corresponding premature failure. As already mentioned, this nanocomposite breaks before reaching the yield point. Although the presence of the clay platelets favors the crystallization in the γ-form, which is more ductile, the clay induced chain immobilization, rather than the crystalline form, appears to play a dominant role in the deformation behavior of the nanocomposites.

During impact testing all the materials under study broke in an instable manner—the total fracture energy was dissipated solely by crack initiation. Figure 5 shows the toughness characterized by the critical J_{Id} value of the *J*-integral as a function of the clay content. It can be seen that toughness is slightly increased by the addition of 1 wt % of the clay. In the case of exfoliated nanocomposites, toughness then decreases with increasing clay content, as the detrimental effect of filler on the failure behavior

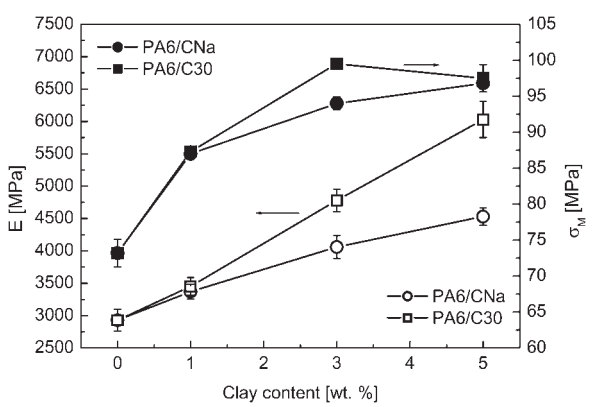

Figure 4 Young modulus, *E*, and tensile strength, σ_M, as a function of the clay content.

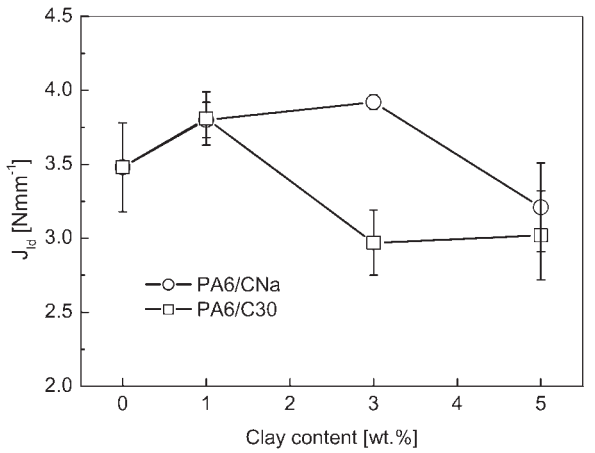

Figure 5 Toughness expressed by the critical *J*-integral value, J_{Id}, as a function of the clay content.

prevails over the positive effect of the γ-phase. For intercalated nanocomposites, the drop in toughness is shifted to higher clay concentration. At the same time, their toughness is systematically higher in comparison with exfoliated nanocomposites. This observation is in good agreement with the behavior observed in static tensile testing. Indeed, the exfoliated structure with a significantly higher amount of confined chains led to higher modulus and strength at the expense of ductility. The transition to brittle behavior with the change from intercalated to exfoliated structures was not compensated by higher amount of γ-phase, which was reported as more ductile than the α-phase.[20] On the other hand, Kim et al.[12] observed higher ductility, that is, higher strain at break and higher Izod impact strength, for polyamide nanocomposites with the exfoliated structure. However, they controlled the clay dispersion in melt-compounded nanocomposites by varying the molecular weight of polyamide matrix. They showed that a large fraction of the γ-phase led to higher density of polymer-clay interaction sites, which provide energetic barrier to interfacial phase separation during deformation. Additionally, the cavitation process inside intercalated tactoids was established as an effective energy dissipation mechanism during deformation.[12] This phenomenon can explain the observed difference in the fracture behavior between intercalated and exfoliated polyamide nanocomposites with the same matrix. The exfoliated nanocomposites contain substantially higher proportions of polymer chains with restricted mobility at the clay surface. As a result, cavitation would take place mainly within intercalated tactoids. Therefore, the fracture toughness of intercalated polyamide nanocomposites is superior to that of exfoliated nanocomposites. Moreover, up to the clay concentration 3 wt %, the toughness of intercalated nanocomposites is higher than that of neat polyamide.

CONCLUSIONS

The effects of the clay dispersion and content on the deformation and fracture behavior of melt-compounded polyamide nanocomposites were investigated. Two nanocomposite systems were evaluated that is, intercalated and exfoliated ones. The clay dispersion was controlled by different nature of the clay surface, that is, by application of sodium-exchanged motmorillonite or organophilized one. It has been shown that while the exfoliated structure imparts higher stiffness and strength to the nanocomposite, the toughness is inferior to that of the intercalated nanocomposite.

References

1. Vaia, R. A.; Giannelis, E. P. MRS Bull 2001, 26, 394.
2. Ray, S. S.; Okamoto, M. Prog Polym Sci 2003, 28, 1539.
3. Alexandre, M.; Dubois, P.; Mater Sci Eng 2000, 28, 1.
4. Zilg, C.; Mulhaupt, R.; Finter, J. J Macromol Chem Phys 1999, 200, 661.
5. Wang, K.; Chen, L.; Wu, J.; Toh, M. L.; He, C.; Yee, A. F. Macromolecules 2005, 38, 788.
6. Kinloch, A. J.; Taylor, A. C. J Mater Sci Lett 2003, 22, 1439.
7. Chen, L.; Wong, S. C.; Pisharath, S. J Appl Polym Sci 2003, 88, 3298.
8. Nathani, H.; Dasari, A.; Misra, R. D. K. Acta Mater 2004, 52, 3217.
9. Gloaguen, J. M.; Lefebvre, J. M. Polymer 2001, 42, 5841.
10. Nair, S. V.; Goettler, L. A.; Lysek, B. A. Polym Eng Sci 2002, 42, 1872.
11. Yu, Z. Z.; Yan, C.; Yang, M.; Mai, Y. W. Polym Int 2004, 53, 1093.
12. Kim, G. M.; Goerlitz, S.; Michler, G. H. J Appl Polym Sci 2007, 105, 308.
13. Lincoln, D. M.; Vaia, R. A.; Wang, Z. G.; Hsiao, B. S.; Krishnamoorti, R. Polymer 2001, 42, 9975.
14. Xiong, M.; Gu, G.; You, B.; Wu, L. J Appl Polym Sci 1923, 2003, 90.
15. Sun, Y.; Zhang, Z.; Moon, K. S.; Wong, C. P. J Polym Sci B 2004, 42, 3849.
16. Park, J.; Jana, S. C. Macromolecules 2003, 36, 8391.
17. Brus, J.; Kelnar, I.; Kotek, J. Macromolecules 2006, 39, 5400.
18. Liu, Z. J.; Chen, K.; Yan, D. Eur Polym Mater 2003, 39, 2359.
19. Sumpter, J. D.; Turner, C. E. Int J Fracture 1973, 9, 320.
20. Ito, M.; Mizuochi, K.; Kanamoto, T. Polymer 1998, 39, 4593.